Journal of Power Sources 189 (2009) 1278–1283

Contents lists available at ScienceDirect

Journal of Power Sources

journal homepage: www.elsevier.com/locate/jpowsour

Fabrication of MnO_2-pillared layered manganese oxide through an exfoliation/reassembling and oxidation process

Jiaqi Yuan[a,b], Zong-Huai Liu[a,b,*], Shanfeng Qiao[a,b], Xiangrong Ma[a,b], Naicai Xu[a,b]

[a] Key Laboratory of Applied Surface and Colloid Chemistry (Shaanxi Normal University), Ministry of Education, Xi'an 710062, PR China
[b] School of Chemistry and Materials Science, Shaanxi Normal University, Xi'an 710062, PR China

ARTICLE INFO

Article history:
Received 14 October 2008
Received in revised form
22 December 2008
Accepted 29 December 2008
Available online 17 January 2009

Keywords:
Pillar
Layered material
Manganese oxide
Delamination/reassembling

ABSTRACT

MnO_2-pillared layered manganese oxide has been first fabricated by a delamination/reassembling process followed by oxidation reaction and then by heat treatment. The structural evolution of MnO_2-pillared layered manganese oxide has been characterized by XRD, SEM, DSC-GTA, IR and N_2 adsorption-desorption. MnO_2-pillared layered manganese oxide shows a relative high thermal stability and mesoporous characteristic. The layered structure with a basal spacing of 0.66 nm could be maintained up to 400 °C. The electrochemical properties of the synthesized MnO_2-pillared layered manganese oxide have been studied using cyclic voltammetry in a mild aqueous electrolyte. Sample MnO_2–BirMO (300 °C) shows good capacitive behavior and cycling stability, and the specific capacitance value is 206 F g^{-1}.

1. Introduction

Pillared inorganic layered nanocomposites are of extensive interest in molecular sieves, selective catalysts, selective absorbents, and lithium battery materials, etc. due to their particular morphologies, structures and properties [1–3]. Typically, pillared inorganic layered nanocomposites are prepared by intercalating guest species into the interlayer of the host inorganic layered materials, followed by calcinations which result in porous architectures in layered inorganic materials [4–6]. In order to increase the thermal stability of the obtained materials and improve their functional properties, robust main-group metal oxides or their mixtures are used as pillaring agents [7].

Layered manganese oxides exhibit excellent cation exchange and molecule adsorptive properties; they can be used as molecular sieves, battery materials, catalysts and precursors to synthesize many porous manganese oxides with tunnel structures [8–10]. Moreover, they can be used to prepare pillared layered manganese oxide with novel functional properties. Up to now, various inorganic pillaring species such as SiO_2, CrOx, $[AlO_4Al_{12}(OH)_{24}(H_2O)_{12}]^{7+}$ (Al_{13} Keggin ion), $Ni(OH)_2$, $LiAl_2(OH)_6$, TiO_2 and $TiO_2 + SiO_2$ have been introduced into the interlayer space of layered manganese oxides by the conventional ion-exchange/intercalation procedure to modify their structures and properties, and resulting pillared layered manganese oxide nanocomposites with various porous structures [11–16]. Experimental results show that the pillaring species obviously affect the porous structure and functional property of the obtained pillared layered inorganic materials. Therefore, developing a new pillaring technology such as MnO_2 as pillaring agent is expected from the viewpoint of probing new functional inorganic materials with novel properties. We tried to prepare MnO_2-pillared layered manganese oxide nanocomposites by the conventional ion-exchange/intercalation procedure, but the result is not ideal.

The exfoliation/reassembling technology of the layered inorganic materials is an efficient way to prepare pillared structure materials with unique physical–chemical properties. Several unique features, such as easy selection of guest species, homogeneous dispersion in the composites, and high surface area associated with a restacked nanoporous nature, can be simply obtained for the prepared pillared structures. Because the delaminated inorganic nanosheets have a higher degree of freedom than the stacked sheets, the guest species can be easily adsorbed on their surface. The pillared layered inorganic nanocomposites can be synthesized through the delamination/reassembling process.

2. Experimental

2.1. Synthesis of MnO_2-pillared layered manganese oxide

The precursor, H-type layered manganese oxide (H-BirMO) was synthesized as reported in the literature [17]. A mixed solution

* Corresponding author at: School of Chemistry and Materials Science of Shaanxi Normal University, Xi'an, Shaanxi 710062, PR China. Tel.: +86 29 85308442; fax: +86 29 85307774.
E-mail address: zhliu@snnu.edu.cn (Z.-H. Liu).

0378-7753/$ – see front matter © 2009 Elsevier B.V. All rights reserved.
doi:10.1016/j.jpowsour.2008.12.148

of 0.6 M NaOH and 2 M H_2O_2 was poured quickly into 0.3 M $Mn(NO_3)_2$ solution and stirred for 25 min. The precipitate was then subjected to hydrothermal treatment at 150 °C for 16 h in a 2 M NaOH solution. The precipitate obtained had a chemical formula of $Na_{0.33}MnO_2{\cdot}0.76H_2O$, which was abbreviated as Na–BirMO. The obtained highly crystallized Na–BirMO was treated with a 0.1 M HCl solution at room temperature for 3 days to produce proton-type layered manganese oxide, which had a chemical formula of $H_{0.27}MnO_2{\cdot}0.67H_2O$ and was abbreviated as H-BirMO.

Delamination of precursor H-BirMO was carried out by the method described in the literature [18]. H-BirMO (0.5 g) was treated in a 0.35 M aqueous solution of tetramethylammonium hydroxide (TMAOH) (125 cm^3) for 7 days at room temperature. The amount of TMAOH added was 25-fold that of the exchangeable capacity of H-BirMO. After soaking, the colloidal suspension was centrifuged at a speed of 13000 rpm for 20 min and washed with 100 cm^3 of distilled water four times to obtain a delaminated BirMO slurry, which contained well-dispersed manganese oxide nanosheets.

The delaminated BirMO slurry was poured into 1 M aqueous solution of $Mn(NO)_3$. The molar ratio of Mn^{2+} ions to the exchangeable capacity of H-BirMO was adjusted to 5. The mixture was maintained overnight while being stirred at room temperature. The product was collected by centrifugation, washed with distilled water, and then dried for 1 day at 50 °C. The Mn^{2+}-intercalated layered manganese oxide was obtained, and it was abbreviated as Mn^{2+}–BirMO. Sample Mn^{2+}–BirMO was then soaked in a mixed solution of $NH_3{\cdot}H_2O + H_2O_2$, maintained overnight at room temperature, MnO_2-pillared layered manganese oxide was obtained, which was abbreviated as MnO_2–BirMO.

Samples Mn^{2+}–BirMO and MnO_2–BirMO were heat-treated in air at different temperatures for 3 h, the obtained materials were abbreviated as MnO_2–BirMO (200), etc., where the number in parentheses is the heating temperature.

2.2. Chemical analyses

The Mn and Na contents of the samples at different stages were determined by atomic absorption spectrometry after they were dissolved in a mixed solution of HCl and H_2O_2.

2.3. Characterization

X-ray diffraction (XRD) analysis was carried out using a D/Max-3c X-ray diffractometer with Cu Kα (λ = 1.5406 Å), using an operation voltage and current of 40 kV and 40 mA, respectively. SEM observation was carried out with a Quanta 200 environmental scanning electron microscope. Infrared spectra were obtained by KBr method on a Fourier Transform Infrared Spectrometer (EQUINX55). TG–DSC curves were obtained on a thermal analyzer (Q1000DSC + LNCS + FACS Q600SDT) at a heating rate of 5 °C min^{-1}. Nitrogen adsorption–desorption at −196 °C was carried out on a Beckman coulter-type apparatus for samples degassed for 4 h below 10^{-3} mmHg. A CHI 600 electrochemical workstation (Chenhua Instrument Co., Shanghai, China) was used for electrochemical measurements.

Electrochemical Measurement: Electrodes were prepared by mixing MnO_2-pillared layered manganese oxide (80 wt%) as active material with acetylene black (15 wt%) and polyvinylidene fluoride (5 wt%). The two first constituents were firstly mixed together to obtain a homogeneous black power. The polyvinylidene fluoride solution (0.02 g mL^{-1}, in N-methyl-ketopyrrolidine) was then added. This resulted in a rubber-like paste, which was brush-coated onto a Ni mesh. The mesh was dried at 110 °C in air for 2 h for the removal of the solvent. After drying, the coated mesh was uniaxially pressed to completely adhere to the electrode material with the current collector.

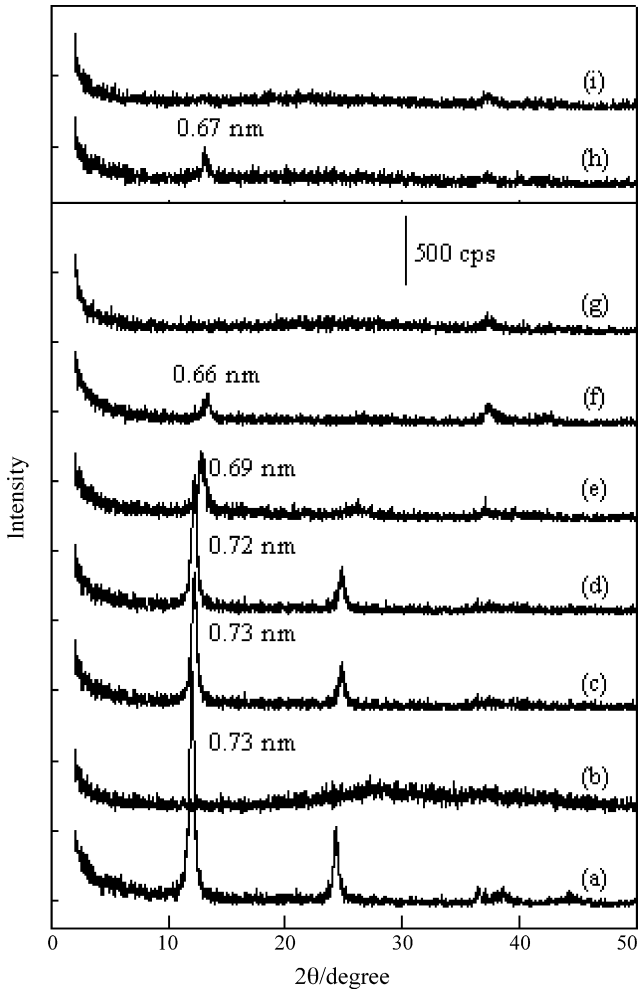

Fig. 1. XRD Patterns of samples obtained at deferent stages: (a) H-BirMO, (b) BirMO slurry, (c) Mn^{2+}–BirMO, (d) MnO_2–BirMO, (e) MnO_2–BirMO (200 °C), (f) MnO_2–BirMO (300 °C), (g) MnO_2–BirMO (400 °C), (h) Mn^{2+}–BirMO (200 °C), and (i) Mn^{2+}–BirMO (300 °C).

A beaker type electrochemical cell equipped with a MnO_2 based working electrode, a Pt-foil (2 cm^2) as the counter electrode and saturated calomel electrode (SCE) as the reference electrode [19]. CV curves were done between −0.2 and 0.8 V in a Na_2SO_4 electrolyte (1.0 mol L^{-1}) at a sweep rate of 5 mV s^{-1}. The average specific capacitance was evaluated from the area of the charge and discharge curves of the CV plot [20].

3. Results and discussion

3.1. The fabrication of MnO_2-pillared layered manganese oxide

The XRD patterns of samples obtained at different stages are shown in Fig. 1. Precursor H-BirMO has a layered structure with a basal spacing of 0.73 nm, with crystal water and exchangeable H^+ ions in the interlayer space (Fig. 1a). The precursor H-BirMO was soaked in a TMAOH solution for 7 days and then washed with distilled water, the obtained BirMO slurry gives no clear peaks but only an amorphous halo (Fig. 1b). The halo can be interpreted as scattering from the nanosheets which are aggregated irregularly, similar to the case of layered titanic acid or graphic oxide [21,22]. This indicates that water washing causes the delamination of stacked layered manganese oxide plates to the individual primary plates [23]. The delaminated BirMO slurry was added to 1 M $Mn(NO_3)_2$ solution at room temperature and stirred for 1 day. After stirring

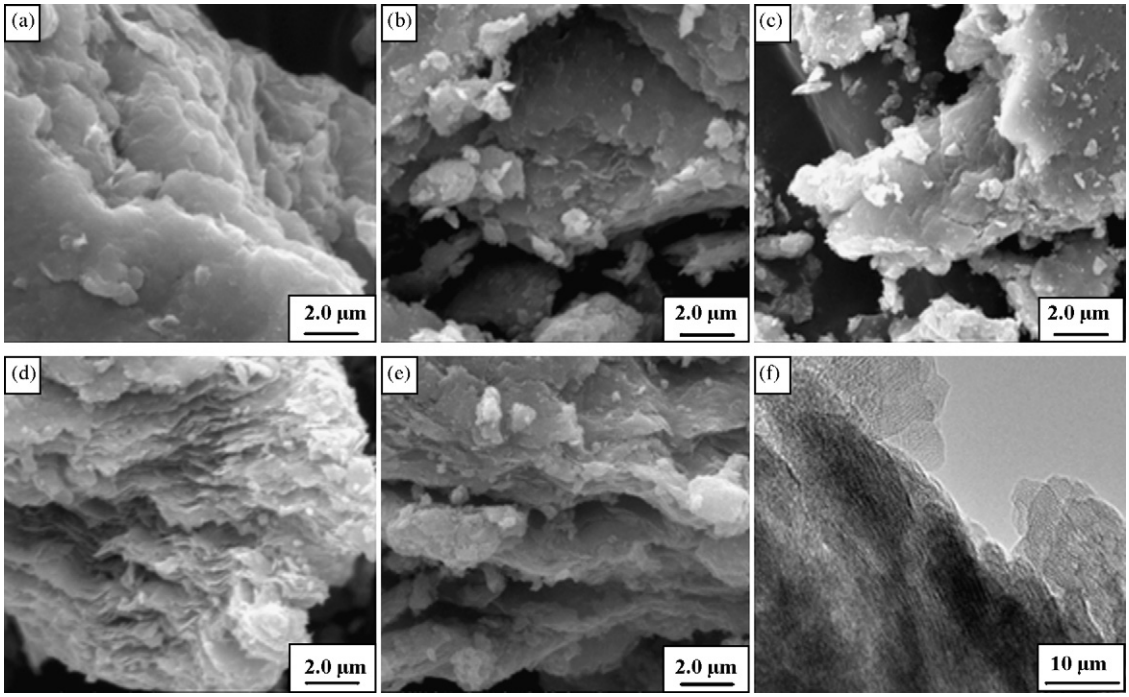

Fig. 2. SEM images of samples at deferent stages: (a) H-BirMO, (b) Mn^{2+}–BirMO, (c) MnO_2–BirMO, (d) MnO_2–BirMO (200 °C), (e) MnO_2–BirMO (300 °C), (f) TEM image of MnO_2–BirMO (300 °C).

and drying at 70 °C for 1 day, sample Mn^{2+}–BirMO still shows a layered structure with a basal spacing of 0.73 nm (Fig. 1c), indicating the reassembling of delaminated sheets progress by only mixing with Mn^{2+} ions followed by air-drying. Since the thickness of MnO_2 nanosheets is known to be about 0.45 nm [18], the gallery height can be calculated as 0.28 nm, being very close to the van der Waals diameter (0.28 nm) of water molecules. This suggests the formation of one molecular layer of water in the interlayer of MnO_2 nanosheets. Because Mn^{2+} ionic radius is 0.08 nm, the intercalated Mn^{2+} ions may randomly exchange with the monolayer water molecules, producing a layered structure of Mn^{2+} intercalated layered manganese oxide, Mn^{2+}–BirMO.

When sample Mn^{2+}–BirMO was soaked in a mixed solution of $NH_3{\cdot}H_2O$ and H_2O_2, the Mn^{2+} ions intercalated in the interlayer of MnO_2 nanosheets are oxidized to MnO_2 particles, and the sample MnO_2–BirMO with a layered structure and a basal spacing of 0.72 nm is obtained (Fig. 1d). MnO_2 particles act as a pillaring agent in the interlayer, which increases the thermal stability of the sample MnO_2–BirMO in comparison with H-BirMO. The layered structure is still maintained even after being heated at 300 °C for 3 h, although both the peak intensity and the basal spacing decrease considerably (Fig. 1f). The layered structure was almost destroyed by being heated at 400 °C (Fig. 1g). On the other hand, sample Mn^{2+}–BirMO was heated at 200 °C for 3 h, the peak intensity and the basal spacing decrease obviously (Fig. 1h). Up to being heated at 300 °C for 3 h, the layered structure was completely destroyed (Fig. 1i). These results indicate that MnO_2 particles as pillaring agents can increase the stability of the layered structure of manganese oxide, and MnO_2-pillared layered manganese oxide nanocomposites are successfully fabricated by a delamination/reassembly and oxidation process and followed by a heating treatment.

3.2. Physical properties

SEM photographs of samples H-BirMO, Mn^{2+}–BirMO and MnO_2–BirMO resemble each other and consist mainly of plate-like particles corresponding to a layered structure (Fig. 2a–c). This indicates that the plate-like form of the precursor H-BirMO is maintained after Mn^{2+} intercalation and MnO_2 pillar into the interlayer of manganese oxide nanosheets. Although the morphology regulation decreases in company with the heating temperature, the layered structure character can be observed for samples MnO_2–BirMO (200 °C) and MnO_2–BirMO (300 °C) due to the function of MnO_2 pillar thermal stability (Fig. 2d and e), which is also supported by TEM image of sample MnO_2–BirMO (300 °C) (Fig. 2f).

IR spectra of samples obtained at different stages in the range of 400–650 cm^{-1} are shown in Fig. 3. Some variations of IR spectra are easily observed. Although bands in the region between 400 and 650 cm^{-1} could be assigned to Mn–O lattice vibration [24,25], the position and intensity of these characteristic adsorbed bands show some obvious changes. In company with the intercalation of Mn^{2+} ions and MnO_2 particles into the interlayer, the bands around 420 and 460 cm^{-1} corresponding to the IR spectrum of the precursor H-BirMO shift to a relative high wavenumber (Fig. 3a and c). Sample MnO_2–BirMO was heat-treated at different temperatures, the Mn–O lattice vibration bands shift to a high wavenumber and an obvious adsorbed band around 532 cm^{-1} is observed due to the Mn–O vibration surrounding change (Fig. 3d and e).

DSC curve of precursor H-BirMO shows a characteristic endothermic peak around 133 °C, which corresponds to the evaporation of the interlayer water and the collapse of the layered structure. The weight loss up to 150 °C is about 13.9% (Fig. 4a). In company with the intercalation of Mn^{2+} ions into the interlayer and followed by oxidation to MnO_2 particles, the endothermic peaks of the evaporation of the interlayer water and the collapse of the layered structure shift to about 152 and 174 °C for samples Mn^{2+}–BirMO and MnO_2–BirMO, respectively. Due to the intercalation of Mn^{2+} ions and MnO_2 particles, the weight loss up to 200 °C decreases to 10.4 and 9.1 %, respectively (Fig. 4b and c). These results imply that the intercalation of Mn^{2+} ions and MnO_2 particles into the interlayer improves the thermal stability of the layered structure. Samples MnO_2–BirMO (200 °C) and MnO_2–BirMO (300 °C) show no obvious endothermic peak corresponding to the collapse of the layered structure because of MnO_2 pillar function (Fig. 4d

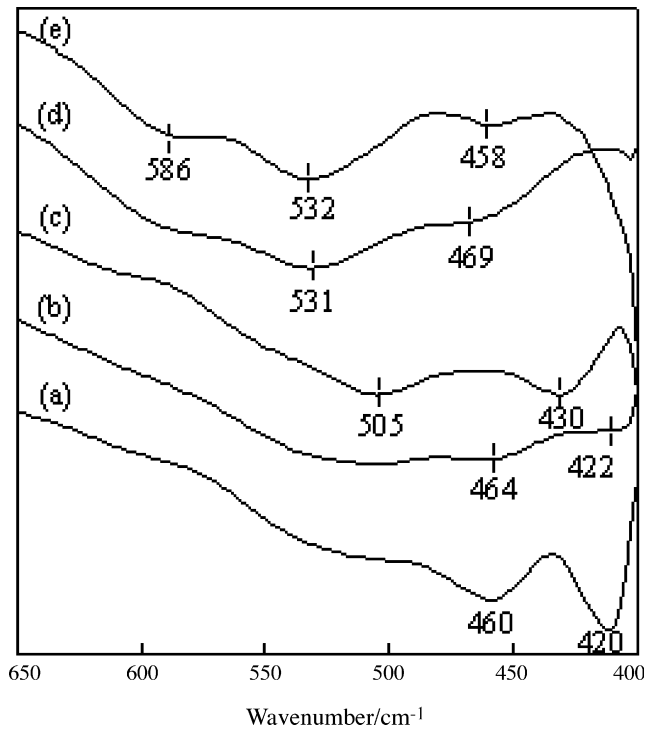

Fig. 3. IR spectra of samples obtained at deferent stages in the range from 400 to 650 cm^{-1}: (a) H-BirMO, (b) Mn^{2+}–BirMO, (c) MnO_2–BirMO, (d) MnO_2–BirMO (200 °C), and (e) MnO_2–BirMO (300 °C).

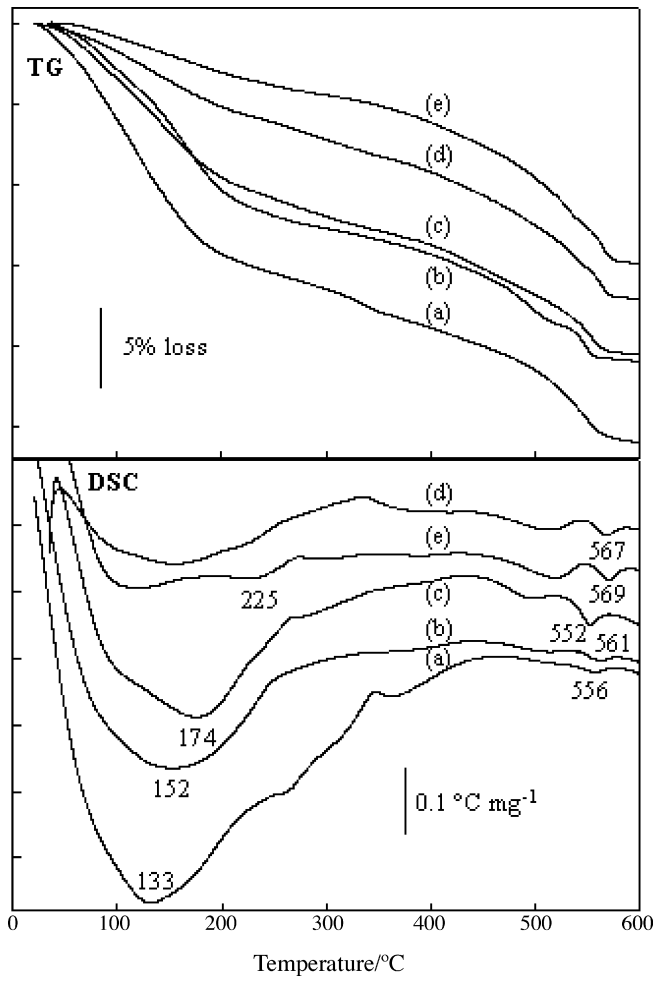

Fig. 4. TG (top) and DSC (bottom) curves of samples obtained at different stages: (a) H-BirMO, (b) Mn^{2+}–BirMO, (c) MnO_2–BirMO, (d) MnO_2–BirMO (200 °C), and (e) MnO_2–BirMO (300 °C).

and e). For all samples, the weight loss around 560 °C is due to the reduction of manganese from tetravalent to trivalent accompanied by the evolution of oxygen for all samples [26].

The porous properties of the samples at different stages have been studied by the nitrogen adsorption–desorption experiment, and the experimental results are shown in Fig. 5. The isotherm for precursor H-BirMO belongs to BDDT type Π with a small hysteresis loop, which corresponds to nonporous or macroporous structures (Fig. 5a). The Brunauer–Emmett–Teller (BET) surface area is about 35 $m^2\,g^{-1}$ (Table 1). These results indicate that the surface area of sample H-BirMO corresponds to the external surface of manganese oxide particles and no micropores are formed in the interlayer. In contrast, the isotherm feature of samples Mn^{2+}–BirMO, MnO_2–BirMO, MnO_2–BirMO (200 °C) and MnO_2–BirMO (300 °C) clearly indicates the presence of mesopores in these samples, classified as type IV as defined by the International Union of Pure and Applied Chemistry (IUPAC) [27]. However, the fraction of mesopores is not so large because the hysteresis loop is not so clear compared with those in typical mesoporous materials [28]. Sample MnO_2–BirMO (200 °C) with layered structure shows a high BET surface area of 116 $m^2\,g^{-1}$ and large N_2 adsorption volume. A *t*-plot analysis confirms the presence of mesopores in sample MnO_2–BirMO (200 °C). The mesoporous surface area is about 102 $m^2\,g^{-1}$, and contributed to about 88% of the total specific

Table 1
Mn content, BET surface area (S_{BET}) and pore volume (V_p) of samples obtained at different stages.

Sample	Mn content (mmol g^{-1})	BET surface area ($m^2\,g^{-1}$)	V_d^p ($cm^3\,g^{-1}$)
H-BirMO	10.51	35	0.19
Mn^{2+}–BirMO	11.18	91	0.33
MnO_2–BirMO	11.76	98	0.34
MnO_2–BirMO (200 °C)	12.48	116	0.35
MnO_2–BirMO (300 °C)	12.61	89	0.38

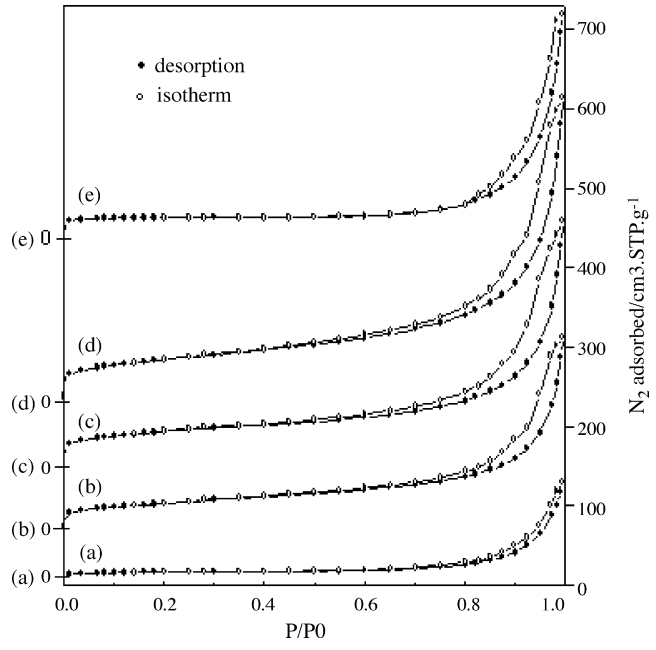

Fig. 5. N_2 adsorption–desorption isotherms of samples obtained at different stages: (a) H-BirMO, (b) Mn^{2+}–BirMO, (c) MnO_2–BirMO, (d) MnO_2–BirMO (200 °C), and (e) MnO_2–BirMO (300 °C).

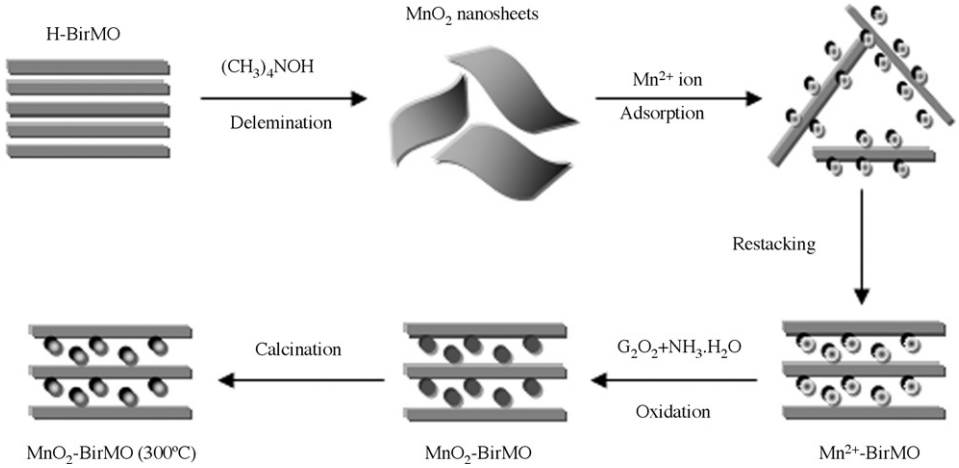

Fig. 6. A model for the formation of MnO_2-pillared layered manganese oxide nanocomposite.

surface area. These results clearly indicate that MnO_2 pillar and followed heat treatment result in the production of mesoporous.

According to the above results, a schematic representation of the structural change during the formation of the MnO_2-pillared layered manganese oxide is given in Fig. 6. The precursor H-BirMO contains one molecular layer of water between the manganese oxide sheets with a basal spacing of 0.73 nm. After the precursor H-BirMO is soaked in 0.35 M TMAOH solution and stirred for 7 days, the intercalation of TMA^+ ions into the interlayer and followed by water washing results in an exfoliation of manganese oxide sheets. When the BirMO slurry of exfoliated MnO_2 nanosheets is soaked in 1 M $Mn(NO_3)_2$ solution, Mn^{2+} ions are adsorbed on the surface of manganese oxide nanosheets. When the suspension is dried at 70 °C, reassembly reaction takes place and Mn^{2+} intercalated layered structure with a basal spacing of 0.73 nm reappears. According to the dimension of manganese oxide layer, the size of water molecules and the radius of Mn^{2+} ions, Mn^{2+} ions may randomly exchange with the water molecules in the interlayer of manganese oxide. After the Mn^{2+}-intercalated layered manganese oxide is treated in a mixed solution of H_2O_2 and $NH_3{\cdot}H_2O$, the intercalated Mn^{2+} ions are oxidized into MnO_2 particles and MnO_2-pillared layered manganese oxide with a basal spacing of 0.72 nm is obtained. MnO_2 pillaring function makes a considerable increase in surface area. Further heat treatment results in the formation of MnO_2-pillared layered manganese oxide nanocomposites with a mesoporous character.

3.3. Electrochemistry property

Manganese oxides with various valence states and crystalline structures are currently investigated for electronic, catalytic and other applications. Extensive studies have shown that manganese oxides are promising electrode materials for electrochemical supercapacitors. Cyclic voltammetry is an important tool to investigate the capacitive behavior of the obtained materials. Fig. 7 shows the first cyclic voltammetry curves for samples MnO_2–BirMO, MnO_2–BirMO (200 °C) and MnO_2–BirMO (300 °C). The CV curves of three samples obtained in a Na_2SO_4 (1.0 mol L^{-1}) solution at a sweep rate of 5 mV s^{-1} show relatively rectangular mirror images with respect to the zero-current line, indicating an obvious capacitive behavior for the obtained materials. Meanwhile, these curves show no peaks, indicating that the electrode capacitor is charged and discharged at a pseudoconstant rate over the complete voltammetric cycle [29,30]. The CV curves of samples MnO_2–BirMO and MnO_2–BirMO (200 °C) electrodes are distorted (Fig. 7a and b), while the one of the sample MnO_2–BirMO (300 °C) electrodes exhibits good symmetrical characteristics (Fig. 7c), suggesting that the reversibility of sample MnO_2–BirMO and MnO_2–BirMO (200 °C) electrodes are not good at this potential range. For sample MnO_2–BirMO (300 °C), the specific capacitance value calculated from the cyclic voltammetry curve is found to be 206 F g^{-1}. The good electrochemical behavior may be ascribed to the relatively high manganese amount and the porous structure.

Electrochemical properties of sample MnO_2–BirMO (300 °C) were more elucidated by CV cyclic voltammetry in a 1 M Na_2SO_4 solution at different potential scan rates ranging from 5 to 50 mV s^{-1}. The current response at the switching potential is distorted by solution and material resistance and this distortion is dependent upon the scan rate. At lower scan rates, the material shows almost ideal capacitive behavior. As the scan rate increases, the deviation from rectangularity of the CV becomes obvious, which can be ascribed to the change of Na^+ ion transplant surrounding (Fig. 8). With a large scan rate, Na^+ ions can only reach the outer surface of the electrode and not enter into the interior pores, and resulting in the capacitance decline.

The cycle performances are of importance for the supercapacitor. The long-term stability of sample MnO_2–BirMO (300 °C) based on as-prepared powder upon cycling was investigated and the variation in specific capacitance over 600 cycles at 10 mV s^{-1} is depicted

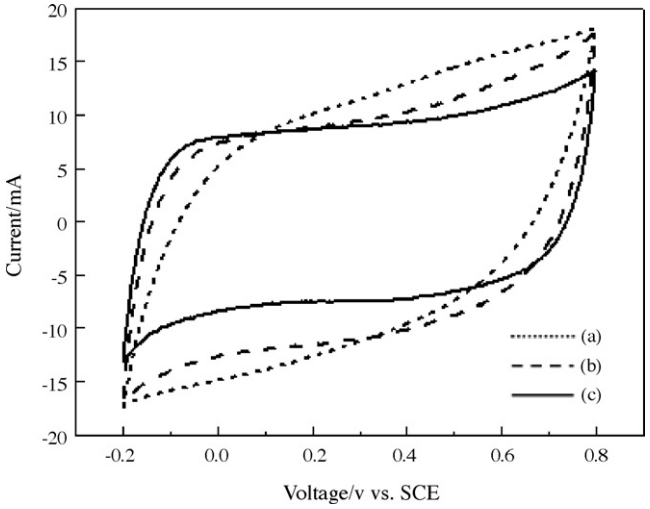

Fig. 7. The first CV curves of samples at different stages at a scan rate of 5 mV s^{-1} in 1 M Na_2SO_4 solution: (a) MnO_2–BirMO, (b) MnO_2–BirMO (200 °C), and (c) MnO_2–BirMO (300 °C).

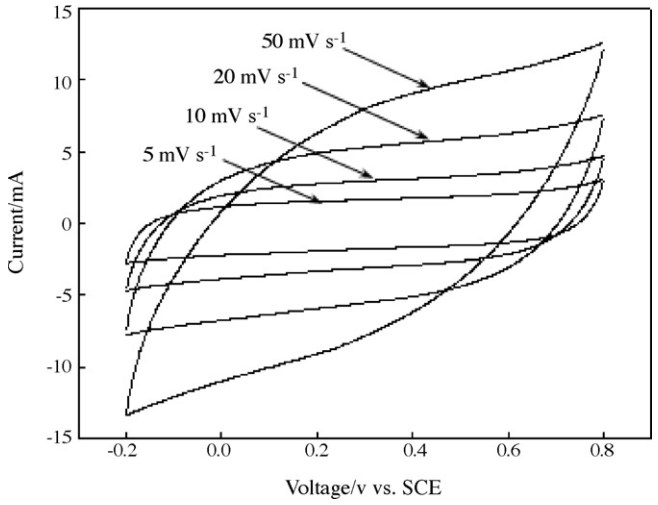

Fig. 8. CV curves of sample MnO_2–BirMO (300 °C) at various scan rate as indicated.

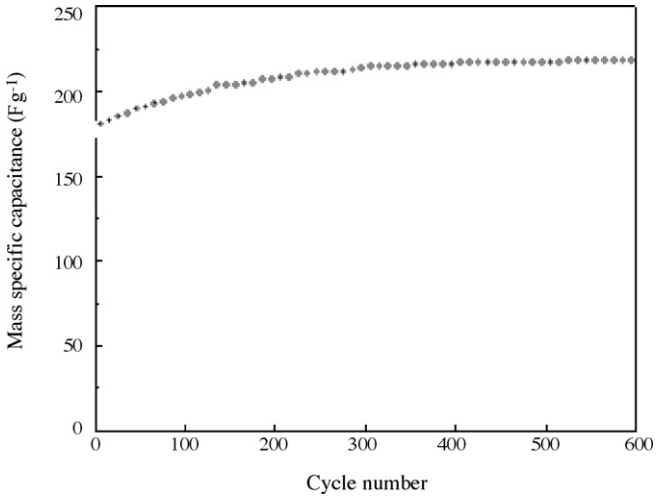

Fig. 9. Variation of specific capacitance of MnO_2–BirMO (300 °C) from 1st to 600th CV cycle at 10 mV s^{-1}.

in Fig. 9. A capacitance increase behavior is observed upon cycling and the capacitance increase remains stable and close to 124% of the starting value after 300 cycles. Similar improvement of the specific capacitance upon cycling has also been reported for MnO_2 thin films [31] and α-MnO_2 [32]. The specific capacitance increase could be attributed to the increase in the active points due to the incomplete intercalation or de-intercalation of the guest ions at relatively high scan rate. The electrode can withstand 600 cycles without significant capacitance loss. This demonstrates that, within the test voltage window, the intercalation and de-intercalation processes of the guest ions do not seem to induce significant structural or meso-structural changes of the electrode as expected for pseudo-capacitive reactions. In comparison with the first curve, the shape of the 600th curves of MnO_2-Bir (300 °C) at 10 mV s^{-1} is more like a rectangle (Supporting information Fig. S1), indicating material MnO_2-Bir (300 °C) has a good cycling stability.

4. Conclusions

We developed a novel synthesis method of pillared layered inorganic materials by a delamination/reassembling process followed by oxidation reaction and then by heat treatment. The synthesized materials had a good thermal stability and mesoporous characteristic, which can be used as active materials for electrochemical supercapacitor. This new synthetic approach could be further expanded to the preparation of various pillared layered inorganic materials with large surface areas, controlled mesoporosity and high thermal stability.

Acknowledgments

We thank National High Technology Research and Development Program of China (2007AA03Z248) and Key Project of the Minister of Education, China for Researching on Science and Technology (106148) for financial support this research.

Supporting Information Available: The first and the 600th CV curves of MnO_2–BirMO (300 °C) at 10 mV s^{-1} are available free of charge via the Internet at http://www.sciencedirect.com.

Appendix A. Supplementary data

Supplementary data associated with this article can be found, in the online version, at doi:10.1016/j.jpowsour.2008.12.148.

References

[1] M. Yanagisawa, S. Uchida, S. Yin, T. Sato, Chem. Mater. 13 (2001) 174–178.
[2] S.-R. Lee, Y.-S. Han, M. Park, G.-S. Park, J.-H. Choy, Chem. Mater. 15 (2003) 4841–4845.
[3] S. Yamanaka, K. Kunii, Z.-L. Xu, Chem. Mater. 10 (1998) 1931–1936.
[4] Z.-H. Liu, X. Yang, K. Ooi, J. Colloid Interface Sci. 265 (2003) 115–120.
[5] Y. Xu, Q. Feng, K. Kajiyoshi, K. Yanagisawa, Chem. Mater. 14 (2002) 697–703.
[6] H.Y. Zhu, Z.H. Zhu, G.Q. Lu, J. Phys. Chem. B 104 (2000) 5674–5680.
[7] Z.-H. Liu, K. Ooi, H. Kanoh, W. Tang, X. Yang, T. Tomida, Chem. Mater. 13 (2001) 473–478.
[8] Q. Feng, H. Kanoh, K. Ooi, J. Mater. Chem. 9 (1999) 319–327.
[9] T.A. Eriksson, Y.J. Lee, J. Hollingsworth, J.A. Reimer, E.J. Cairns, X.-F. Zhang, M.M. Doeff, Chem. Mater. 15 (2003) 4456–4463.
[10] O. Giraldo, S.L. Brock, W.S. Willis, M. Marquez, S.L. Suib, S. Ching, J. Am. Chem. Soc. 122 (2000) 9330–9331.
[11] Y. Ma, S.L. Suib, T. Ressler, J. Wong, M. Lovallo, M. Tsapatsis, Chem. Mater. 11 (1999) 3545–3554.
[12] F. Zhang, K. Ngala, M.S. Whittingham, Electrochem. Commun. 2 (2000) 445–447.
[13] Y. Xu, Q. Feng, K. Kajiyoshi, K. Yanagisawa, X. Yang, Y. Makita, S. Kasaishi, K. Ooi, Chem. Mater. 14 (2002) 3844–3851.
[14] L. Wang, Y. Ebina, K. Takada, K. Kurashima, T. Sasaki, Adv. Mater. 16 (2004) 1412–1416.
[15] Z.-H. Liu, X. Tang, C. Zhang, Q. Zhou, Chem. Lett. 34 (2005) 1312–1313.
[16] J. Wang, Z.-H. Liu, X. Tang, K. Ooi, J. Colloid Interface Sci. 307 (2007) 524–530.
[17] L. Liu, Q. Feng, K. Yanagisawa, Yi. Wang, J. Mater. Sci. Lett. 19 (2000) 1567–1570.
[18] Z.-H. Liu, X. Yang, Y. Makita, K. Ooi, Chem. Mater. 14 (2002) 4800–4806.
[19] V. Subramanian, H. Zhu, B. Wei, J. Power Sources 159 (2006) 361–364.
[20] C.-Z. Yuan, B. Gao, X.-G. Zhang, J. Power Sources 173 (2007) 606–612.
[21] R. Schollhorn, Chem. Mater. 8 (1996) 1747–1757.
[22] T. Sasaki, M. Watanabe, J. Am. Chem. Soc. 120 (1998) 4682–4689.
[23] Z.-H. Liu, K. Ooi, H. Kanoh, W. Tang, T. Tomida, Langmuir 16 (2000) 4154–4164.
[24] X. Yang, Y. Makita, Z. Liu, K. Sakane, K. Ooi, Chem. Mater. 16 (2004) 5581–5588.
[25] J. Luo, A. Huang, S.H. Park, S.L. Suib, C.-L. O'Young, Chem. Mater. 10 (1998) 1561–1568.
[26] C. Gonzdlez, J.L. Gutierrez, J.R. Gonzalez-Velasco, A. Cid, A. Arranz, J.F. Arranz, J. Therm. Anal. 47 (1996) 93–102.
[27] G. Andoni, G. Garbine, G. Paul, M. Mario, J. Phys. Chem. 99 (1995) 301–312.
[28] Z.-M. Wang, Z. Liu, N. Yamashita, H. Kanoh, K. Ooi, Langmuir 18 (2002) 1957–1962.
[29] M. Toupin, T. Brousse, D. Belanger, Chem. Mater. 14 (2002) 3946–3952.
[30] X. Zhang, W. Yang, D.G. Evans, J. Power Sources 184 (2008) 695–700.
[31] S.C. Pang, M.A. Anderson, T.W. Chapman, J. Electrochem. Soc. 147 (2000) 444–450.
[32] M. Toupin, T. Brousse, D. Bélanger, Chem. Mater. 14 (2002) 3946–3952.